The Astrophysical Journal, 637:486–493, 2006 January 20

A MASSIVE JET EJECTION EVENT FROM THE MICROQUASAR SS 433 ACCOMPANYING RAPID X-RAY VARIABILITY

T. Kotani,[1] S. A. Trushkin,[2] R. Valiullin,[3] K. Kinugasa,[4] S. Safi-Harb,[5] N. Kawai,[1] and M. Namiki[6]
Received 2005 June 6; accepted 2005 September 21

ABSTRACT

Microquasars occasionally exhibit massive jet ejections that are distinct from the continuous or quasi-continuous weak jet ejections. Because these massive jet ejections are rare and short events, they have hardly been observed in X-rays so far. In this paper, the first X-ray observation of a massive jet ejection from the microquasar SS 433 with the *Rossi X-Ray Timing Explorer* (*RXTE*) is reported. SS 433 undergoing a massive ejection event shows a variety of new phenomena, including a QPO-like feature near 0.1 Hz, rapid time variability, and shotlike activities. The shotlike activity may be caused by the formation of a small plasma bullet. A massive jet may consist of thousands of such plasma bullets ejected from the binary system. The size, mass, internal energy, and kinetic energy of the bullets and the massive jet are estimated.

Subject headings: X-rays: binaries — X-rays: individual (SS 433)

1. INTRODUCTION

Microquasars are stellar X-ray binaries (neutron stars or black holes) from which relativistic jets emanate via an unknown, very efficient mechanism (Mirabel & Rodríguez 1999). Microquasars such as SS 433 and GRS 1915+105 occasionally exhibit massive jet ejections, which are recognized as sporadic flares in their radio light curves (Fiedler et al. 1987; Foster et al. 1996). Because the massive jet ejections are rare (a few per year), short (within a few days), and aperiodic, pointing X-ray observations of these events have hardly been performed so far. As for SS 433, no X-ray observation has been confirmed to coincide with a radio flare, except for one or two possible coincident observations with *Einstein* in 1979 (Band 1989). A monitoring observation over 10 days and a long-look observation lasting 13 days were performed with *ASCA* (*Advanced Satellite for Cosmology and Astrophysics*) in 1995 and 2000 (Kotani 1997; Namiki et al. 2001), respectively, but there was no radio flare coinciding with these periods. A multiwavelength observation with the *Rossi X-Ray Timing Explorer* (*RXTE*) and the Giant Meter Radio Telescope in 2002 also missed radio flares (Chakrabarti et al. 2003). It should be stressed that the massive jets are distinct from the stable continuous jets of SS 433 and the quasi-continuous or weak jet of GRS 1915+105. The radio activity of SS 433 monitored by the Green Bank Interferometer over several years may be characterized as a clustering of flare events separated by periods of quiescent emission (Fiedler et al. 1987). In these sporadic radio flare events, the radio flux density at 2.3 GHz exceeds 1 Jy, and massive jet blobs, which are recognized as bright extended spots in radio images, are ejected from the core of SS 433 at one-quarter of the speed of light (Vermeulen et al. 1993). The ejection of massive jet blobs from GRS 1915+105 with a radio flux exceeding 100 mJy, by which the source was recognized as a microquasar in the first place (Mirabel & Rodríguez 1994; Fender 2001), has hardly been observed in X-rays (Muno et al. 2001), in contrast to a number of reports on the X-ray observation of the quasi-continuous or weak jet ejections (Mirabel et al. 1998; Klein-Wolt et al. 2002; Ueda et al. 2002).

We report on a successful X-ray observation of a massive jet ejection from SS 433 with *RXTE*. The observation scheme is described in § 2, and the data are analyzed and discussed in § 3.

2. OBSERVATIONS

Formerly, a radio flare was the only indicator of a massive jet ejection. Unfortunately, an X-ray observation triggered by a radio flare is too late to catch the moment of the ejection, as experienced in the cases of several previous target-of-opportunity (ToO) X-ray observations. Because the X-ray activity precedes a radio flare, a ToO X-ray observation will not work for a massive jet ejection event. So we have built a strategy to observe a *second* massive jet ejection event following the first event. In the active state of SS 433, radio flares are clustered with an interval of 8–23 days (Fiedler et al. 1987). Therefore, a series of monitoring observations triggered by a massive jet ejection may cover the moment of a second ejection within 23 days.

We planned a 30 day long ToO monitoring observation of SS 433 with *RXTE* to be triggered by a radio flare. The proposal was accepted in Cycle 6 of the *RXTE* Guest Observer Program carried out for 1 yr beginning in 2001 March. The daily radio activity of the source has been monitored with the RATAN-600 radio telescope (Korolkov & Pariiskii 1979) of the Special Astrophysical Observatory of the Russian Academy of Sciences (SAO RAS) since 2001 September. After 2 months of static activity with an average flux density of 0.7 Jy at 2.3 GHz, a significant flare occurred on 2001 November 2 (MJD = 52,215), indicating that the source entered its active state (Fig. 1). Flux densities reached 1.3 Jy at 2.3 GHz on MJD = 52,216.6 (Kotani & Trushkin 2001; Trushkin et al. 2003). We started a series of X-ray observations with *RXTE* on MJD = 52,222 (Kotani et al. 2003; Safi-Harb & Kotani 2003). Except for a break at MJD = 52,231, SS 433 was observed for 3 ks every day. In the X-ray light curve, a temporal variation with timescales of 10–100 s appeared on MJD = 52,225, and the amplitude increased day by day (Fig. 3). On MJD = 52,232, the amplitude reached a maximum, and the 2–10 keV X-ray flux reached a local maximum of 2.5×10^{-10} ergs s^{-1} cm^{-2}. The X-ray emission, thought to originate in the hot part of the jets as long as or longer than 10^{12} cm,

[1] Tokyo Tech, 2-12-1 O-okayama, Tokyo 152-8551, Japan; kotani@hp.phys.titech.ac.jp.
[2] Special Astrophysical Observatory RAS, Nizhnij Arkhyz, Karachaevo-Cherkassia 369167, Russia.
[3] Astrophysical Institute of Kazakh Academy of Sciences, 480020 Alma Ata, Kazakhstan.
[4] Gunma Astronomical Observatory, 6860-86 Nakayama, Takayama, Agatsuma, Gunma 377-0702, Japan.
[5] University of Manitoba, Winnipeg, MB R3T 2N2, Canada.
[6] Osaka University, 1-1 Machikaneyama, Toyonaka, Osaka 560-0043, Japan.

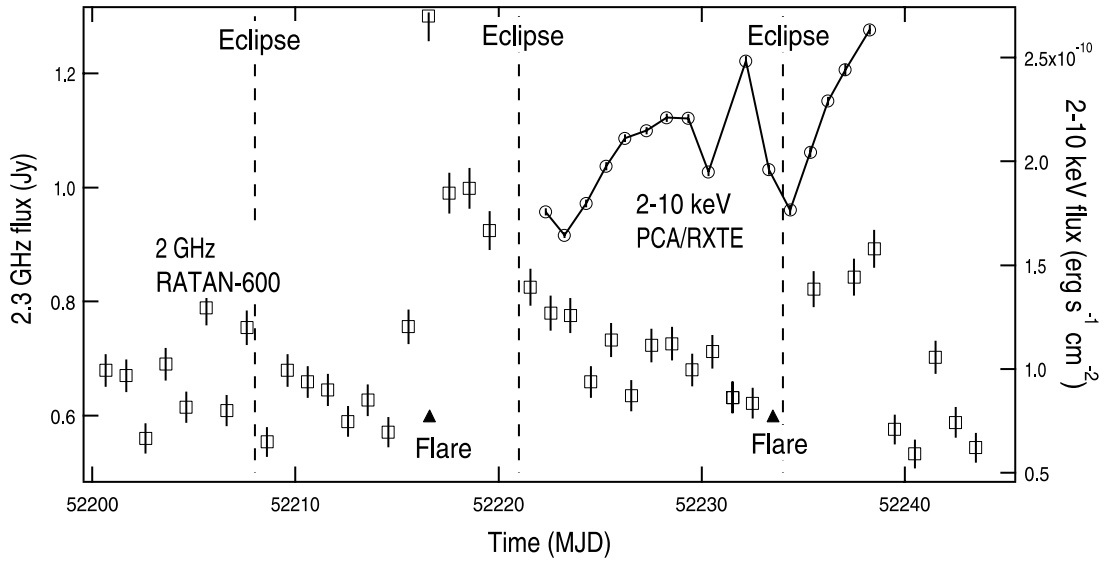

FIG. 1.—2.3 GHz radio light curve (*squares with error bars*) and 2–10 keV X-ray light curve (*circles with error bars and solid line*) of SS 433. The radio flux taken with RATAN-600 shows two flares, or massive jet-blob ejections, indicated by filled triangles. The epochs of eclipse are indicated by dashed lines. The first flare triggered *RXTE* monitoring observations. The rise of the second flare is not prominent because of a lack of monitoring data on MJD = 52,234 due to bad weather conditions. The X-ray fluxes show a peak just before the second radio flare and then a dip coinciding with an eclipse.

had never shown such a variability in past observations (Safi-Harb & Kotani 2003). Following the maximum of the flux and the variation amplitude, a second radio flare was detected on MJD = 52,235. Due to a missing radio data point at MJD = 52,234, the precise onset time and peak flux of the second flare are unfortunately not known, but they are not likely out of the range 52,233 < MJD ≤ 52,235 and 1.5 Jy < F < 2 Jy. Thus, we conclude that the moment of a massive jet ejection was observed in the X-ray band. After the peak, the X-ray flux dropped due to a binary eclipse. The X-ray monitoring observation lasted until MJD = 52,238, for 17 days, providing 16 data sets. An observation log is shown in Table 1. Optical spectroscopic observations were performed on MJD = 52,220.6, 52,221.6, and 52,225.6 with the 0.7 m telescope at the observatory Kamenskoe Plato (Mironov & Tereshchenko 1998) and on MJD = 52,229.39 and 52,233.38 with the 0.65 m telescope at the Gunma Astronomical Observatory (Hasegawa et al. 2004; Kinugasa et al. 2002). Based on the spectroscopic data, the variation of the Doppler shifts of the jets during the campaign are estimated. The Doppler parameter of the receding jet is estimated to increase from 0.07 on MJD = 52,222 to 0.13 on 52,238, and that of the approaching jet to decrease from −0.02 to −0.07.

3. DATA ANALYSIS AND DISCUSSION

3.1. *The QPO-like Feature*

First, we have searched for a periodicity in the data. No coherent pulsation has been detected from the 16 data sets, but a feature that can be interpreted as a quasi-periodic oscillation (QPO) has been found at 0.1 Hz in the sum of the 16 power density spectra. The sum of the power density spectra is shown in Figure 2. The fraction of the flux accounting for the QPO-like variation is estimated from the ratio of the Gaussian normalization to the area under the power-law continuum.

TABLE 1
OBSERVATION LOG

Date (2001)	Start (MJD)	End (MJD)	Exposure Time (ks)	PCU[a]
Nov 9	07:10 (52,222.299)	08:11 (52,222.341)	3.6	0234
Nov 10	05:19 (52,223.222)	06:21 (52,223.265)	3.7	0234
Nov 11	06:47 (52,224.283)	07:47 (52,224.325)	3.6	0234
Nov 12	06:35 (52,225.275)	07:35 (52,225.316)	3.5	0234
Nov 13	04:46 (52,226.199)	05:46 (52,226.240)	3.5	0234
Nov 14	06:11 (52,227.258)	07:13 (52,227.301)	3.7	0234
Nov 15	06:00 (52,228.250)	07:01 (52,228.293)	3.7	0234
Nov 16	07:26 (52,229.310)	08:32 (52,229.356)	4.0	023
Nov 17	07:14 (52,230.302)	08:20 (52,230.349)	4.1	023
Nov 19	03:41 (52,232.154)	04:33 (52,232.190)	3.1	0234
Nov 20	06:40 (52,233.278)	07:46 (52,233.324)	4.0	02
Nov 21	08:05 (52,234.337)	09:16 (52,234.387)	4.3	023
Nov 22	07:54 (52,235.330)	09:05 (52,235.379)	4.2	024
Nov 23	04:32 (52,236.189)	05:29 (52,236.229)	3.5	024
Nov 24	01:11 (52,237.050)	01:54 (52,237.080)	2.6	02
Nov 25	05:45 (52,238.240)	06:47 (52,238.283)	3.7	012

[a] Proportional counter units in operation.

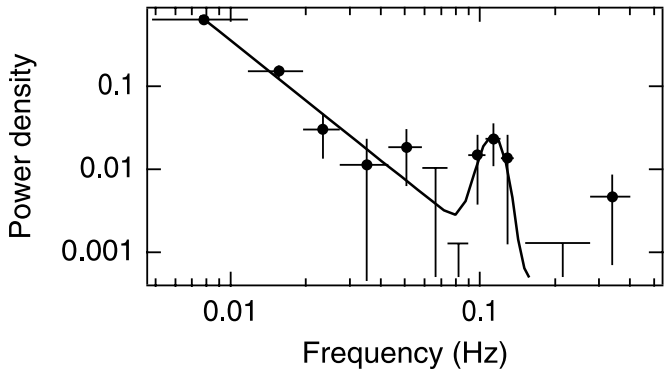

FIG. 2.—Sum of power density spectra of the X-ray data. The sum of all 16 spectra and the best-fit model of a power-law model plus a Gaussian (*solid line*) are plotted. The data points and upper limits are marked as filled circles and T-shaped bars, respectively. A feature that can be interpreted as a QPO centered at 0.1127 ± 0.0072 Hz with a Gaussian σ of 0.011 ± 0.006 Hz is seen.

This is the first detection of any periodicity or quasi periodicity shorter than 1 day from this source. Interestingly, other microquasars such as GRS 1915+105 also show 0.5–10 Hz low-frequency QPOs, which are considered to represent a characteristic timescale in the accretion flow (Muno et al. 2001). A supercritical accretion flow, which SS 433 is believed to have, had not been observed in the X-ray band because of the bright jets. The 0.1 Hz QPO-like feature may be the first detection of the supercritical accretion flow or disk in the X-ray band. The similarity to the QPO in other microquasars suggests the presence of a common mechanism working in other systems and SS 433, at least when the latter is undergoing a massive jet ejection.

3.2. *Spectral Fitting*

The 16 data sets have been reduced with the standard reduction method.[7] The spectra are fitted with an empirical model,

$$e^{-\sigma(E)N_{\rm H}} \times [\text{bremsstrahlung}(kT) + F_N \times \text{narrow-line}(E_N, \sigma_N) + F_B \times \text{broad-line}(E_B, \sigma_B)], \quad (1)$$

[7] See *RXTE* GOF, http://heasarc.gsfc.nasa.gov/docs/xte/xhp_proc_analysis.html.

where $\sigma(E)$ is the absorption cross section, F_N and F_B are line fluxes, E_N and E_B are line center energies, and σ_N and σ_B are line widths. The hydrogen column density $N_{\rm H}$ and the width of the narrow line σ_N are fixed to 6×10^{21} cm^{-2} and 0 keV, respectively. The results are shown in Table 2. The model has been applied to SS 433's spectra obtained with the Large Area Counter (LAC) on board *Ginga* (Kawai 1989; Yuan et al. 1995), a proportional counter array whose energy resolution and energy band are similar to those of the PCA on board *RXTE*. This model is a simple approximation of the complicated, line-abundant spectrum revealed with the finer energy resolutions of *ASCA* SIS (Kotani et al. 1996) and *Chandra* HETGS (Marshall et al. 2002). In this model, the Doppler-shifted pairs of Fe XXV Kα, Fe XXVI Kα, and Ni XXVII Kα lines are blended into the "narrow" and "broad" iron lines. The parameters that cannot be determined from an *RXTE* spectrum, such as line flux ratios Fe XXVI/Fe XXV and red/blue, are naturally eliminated from the model. The average spectrum of each data set and its evolution can be reproduced with the model and the spectral parameters in Table 2, together with the 2–10 keV fluxes in Figure 1.

In the eclipse at MJD = 52,234, both the bremsstrahlung temperature and the line fluxes drop, as observed with *Ginga* LAC (Kawai 1989; Yuan et al. 1995). The equivalent widths of the two lines at the flux maximum (MJD = 52,232) and the eclipse (MJD = 52,234) are 1.76 and 1.56 keV, respectively. The equivalent width is not sensitive to eclipse because the base of the jet, which is responsible for both the Doppler-shifted line emission and the continuum emission, is occulted in eclipse (Kawai 1989; Yuan et al. 1995; Gies et al. 2002).

3.3. *The Rapid Variability*

3.3.1. *Data Analysis*

Then we examined the rapid variation seen on MJD = 52,232 (Fig. 3). The variation, which might appear irregular or chaotic, can be interpreted as a series of "shots" or "spikes" with widths of tens of seconds. Their intervals are random and do not show any periodicity. We have sampled 12 shots as indicated in Figure 3 and folded the light curve to make the average profile of the shots (Fig. 4). The shot rises fast then slightly softens

TABLE 2
SPECTRAL PARAMETERS

Start (MJD)	kT (keV)	E_N (keV)	F_N ($\times 10^{-4}$ photons s^{-1} cm^{-2})	E_B (keV)	σ_B (keV)	F_B ($\times 10^{-3}$ photons s^{-1} cm^{-2})	χ^2/dof
52,222.299	35 ± 2	6.5 ± 0.1	5.1 ± 1.4	6.92 ± 0.06	0.83 ± 0.07	2.2 ± 0.2	30.5/31
52,223.222	49 ± 3	6.4 ± 0.1	4.7 ± 1.2	6.98 ± 0.06	0.81 ± 0.10	2.2 ± 0.1	51.5/31
52,224.283	47 ± 3	6.5 ± 0.1	4.7 ± 1.5	6.98 ± 0.08	0.83 ± 0.05	2.2 ± 0.2	29.7/31
52,225.275	56 ± 5	6.7 ± 0.1	5.2 ± 1.4	6.95 ± 0.06	1.00 ± 0.07	2.9 ± 0.2	57.0/31
52,226.199	55 ± 4	6.7 ± 0.1	6.5 ± 1.2	6.90 ± 0.05	1.07 ± 0.07	3.1 ± 0.1	82.8/31
52,227.258	45 ± 2	6.8 ± 0.1	5.5 ± 1.2	6.90 ± 0.05	1.10 ± 0.05	3.1 ± 0.2	45.0/31
52,228.250	37 ± 2	6.8 ± 0.1	4.8 ± 1.5	6.92 ± 0.06	0.99 ± 0.07	2.8 ± 0.1	39.9/31
52,229.310	48 ± 3	6.8 ± 0.1	6.3 ± 1.4	6.94 ± 0.05	1.07 ± 0.05	2.9 ± 0.2	38.7/31
52,230.302	37 ± 2	6.9 ± 0.2	3.4 ± 1.4	6.97 ± 0.05	0.95 ± 0.05	2.3 ± 0.2	49.6/31
52,232.154	38 ± 2	7.0 ± 0.1	5.9 ± 1.1	6.88 ± 0.06	1.21 ± 0.08	3.3 ± 0.2	72.2/31
52,233.278	25 ± 1	7.0 ± 0.2	2.2 ± 1.4	7.06 ± 0.07	0.93 ± 0.08	2.0 ± 0.2	87.1/30
52,234.337	21 ± 1	6.8 ± 0.4	2.2 ± 1.2	7.11 ± 0.08	1.07 ± 0.06	2.1 ± 0.2	42.1/30
52,235.330	48 ± 3	7.0 ± 0.1	6.0 ± 1.3	6.88 ± 0.08	1.12 ± 0.11	2.5 ± 0.2	38.4/30
52,236.189	53 ± 4	7.0 ± 0.1	5.1 ± 1.5	6.92 ± 0.07	1.05 ± 0.10	2.7 ± 0.2	53.1/30
52,237.050	55 ± 5	7.0 ± 0.1	6.6 ± 1.2	6.74 ± 0.10	1.24 ± 0.13	3.0 ± 0.3	51.9/30
52,238.240	42 ± 2	7.1 ± 0.1	6.9 ± 1.0	6.92 ± 0.07	1.27 ± 0.06	3.4 ± 0.2	42.9/30

NOTE.—For 2–10 keV flux, see Fig. 1.

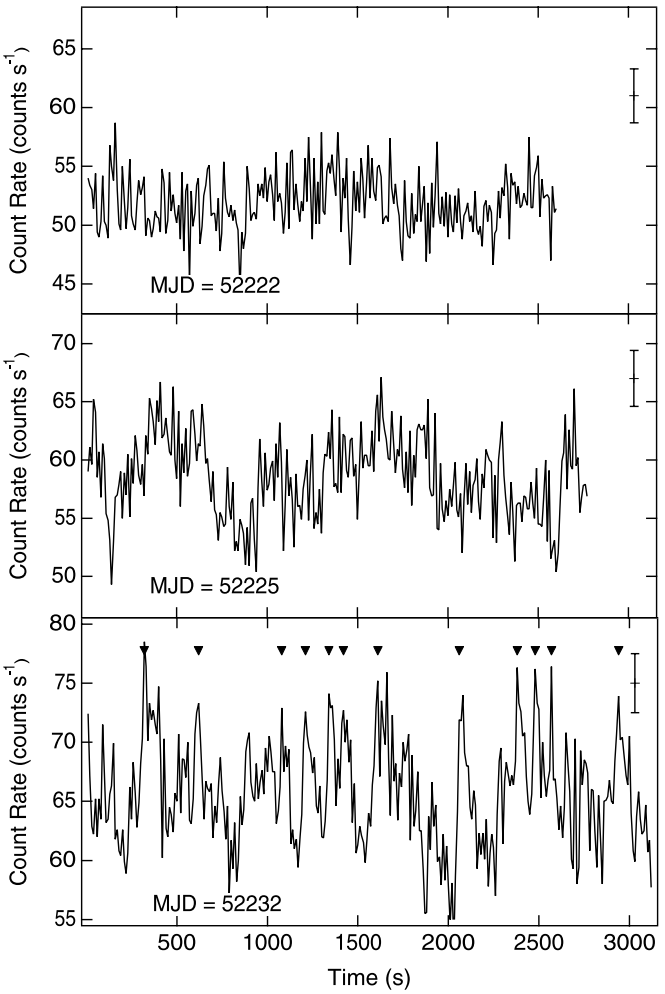

FIG. 3.—Blown-up X-ray light curves taken on MJD = 52,222 (*top*), 52,225 (*middle*), and 52,232 (*bottom*). Only the energy band higher than the iron and nickel lines (8.38 keV for blueshifted Ni XXVII Kα) is shown. Typical 1 σ errors are plotted as crosses. The amplitude of variations on MJD = 52,222, if any, is not larger than the error bar. On MJD = 52,225, the variations become significant, and the amplitude reaches maximum on 52,232. The variation on MJD = 52,232 can be interpreted as a series of "shots" or "spikes." By picking up local maxima in the light curve above a threshold of 74 counts s^{-1} after at least two successive increasing bins (30 s), 12 shots are sampled as indicated by the filled triangles in the bottom panel. The criterion of successive increasing bins is necessary to cut local maxima due to fluctuation. The threshold of 74 counts s^{-1} (13 σ) is chosen so that most shots are sampled only once. This sampling is not exhaustive, and a different set of shots may be selected under another criterion.

during the decay. The 8.4–21 keV profile is fitted with a burst model,

$$\text{constant} + A \times \begin{cases} 0, & t \le t_0, \\ (t - t_0)/-t_0, & t_0 \le t \le 0, \\ \exp(-t/\tau_{\rm dec}), & 0 \le t, \end{cases} \qquad (2)$$

where A is a normalization factor, t is the time from the peak, t_0 is the time of the onset of the shot, and $\tau_{\rm dec}$ is the decay timescale. The onset time and decay timescale are fitted to be -23^{+5}_{-4} and 41^{+12}_{-9} s, respectively.

We have divided the profile into three phases, namely, the "preshot" phase, the "peak" phase, and the "decay" phase, and made a spectrum from each phase. We have subtracted the preshot spectrum from the peak spectrum and from the decay spectrum to extract the pure shot component. The pure shot component is

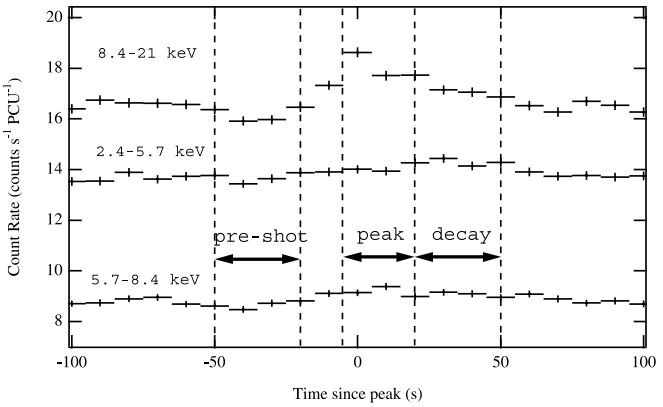

FIG. 4.—Average profile of the 12 shots sampled from the data on MJD = 52,232 (Fig. 3). In the 8.4–21 keV band, the shot rises in $\sim$10 s and decays slowly ($\sim$30 s). In the 2.4–5.7 keV band, the profile is less pronounced: the peak lags behind that in the hard band by $\sim$30 s, and both the rise and decay timescales are $\sim$30 s. The peak is indistinct in the 5.7–8.4 keV band as well. That implies that the iron line intensity does not contribute much to the shot. For a spectroscopic study, we have divided the profile into three phases: the "preshot," "peak," and "decay" phases.

shown in Figure 5, together with the preshot spectrum. The 3–20 keV fluxes in the peak and decay phases are 1.9×10^{-10} and 5.7×10^{-11} ergs s^{-1} cm^{-2}, respectively. The shot component is well fit by either an absorbed power-law model or an absorbed thermal bremsstrahlung model. No emission line is detected. The total spectrum integrated over all data taken on MJD = 52,235 is expressed as an attenuated bremsstrahlung model and requires the addition of a broad iron line of 7.00 ± 0.02 keV. The hydrogen column density decreases in the decay phase from $60^{+50}_{-32} \times 10^{22}$ to $18^{+20}_{-13} \times 10^{22}$ cm^{-2} in both models used to fit the data. The best-fit thermal bremsstrahlung temperature and power-law photon index at the peak are $kT_1 = 14^{+86}_{-9}$ keV and $1.6^{+0.3}_{-0.3}$, respectively. Neither the index nor the temperature changes significantly during the decay. The unabsorbed 2–10 keV luminosity at the peak is fitted to be $L_1 = 4.7^{+1.5}_{-1.9} \times 10^{35}$ ergs s^{-1} assuming a distance of $D = 4.85$ kpc (Vermeulen et al. 1993).

3.3.2. *Interpretation*

This is the first detection of a rapid X-ray variability with a timescale less than 300 s from SS 433 (Kotani et al. 2002, 2003; Safi-Harb & Kotani 2003). Although this source had been observed numerous times by various X-ray observatories, only variability with timescales $\ge$1 day had been reported. For example, *Einstein* observed the source to vary by a factor of 2 on timescales of 1 day (Band 1989), and daily variations other than the orbital and precessional modulations are seen in *Ginga* and *ASCA* data (Yuan et al. 1995; Kotani 1997). Temporal analysis of *ROSAT* (*Röntgensatellit*) data shows flickering around 3–10 s, but this variability does not appear consistently (Safi-Harb 1997). Since the detection with *RXTE* in 2001 (Kotani et al. 2002, 2003; Safi-Harb & Kotani 2003), evidence of rapid X-ray variability has been accumulated. Chakrabarti et al. (2003) report on X-ray variability with timescales of a few minutes detected in 2002 with *RXTE*, and Revnivtsev et al. (2004) detected a significant X-ray variability with timescales as short as 100 s with *RXTE* in 2004.

The absence or weakness of a rapid X-ray variability had been explained in terms of an X-ray–emitting jet of length $\ge 10^{12}$ cm. Together with the QPO-like feature in the power density spectrum, this shotlike variability implies the presence of X-ray sources smaller than 10^{12} cm in the system. Considering that these shots

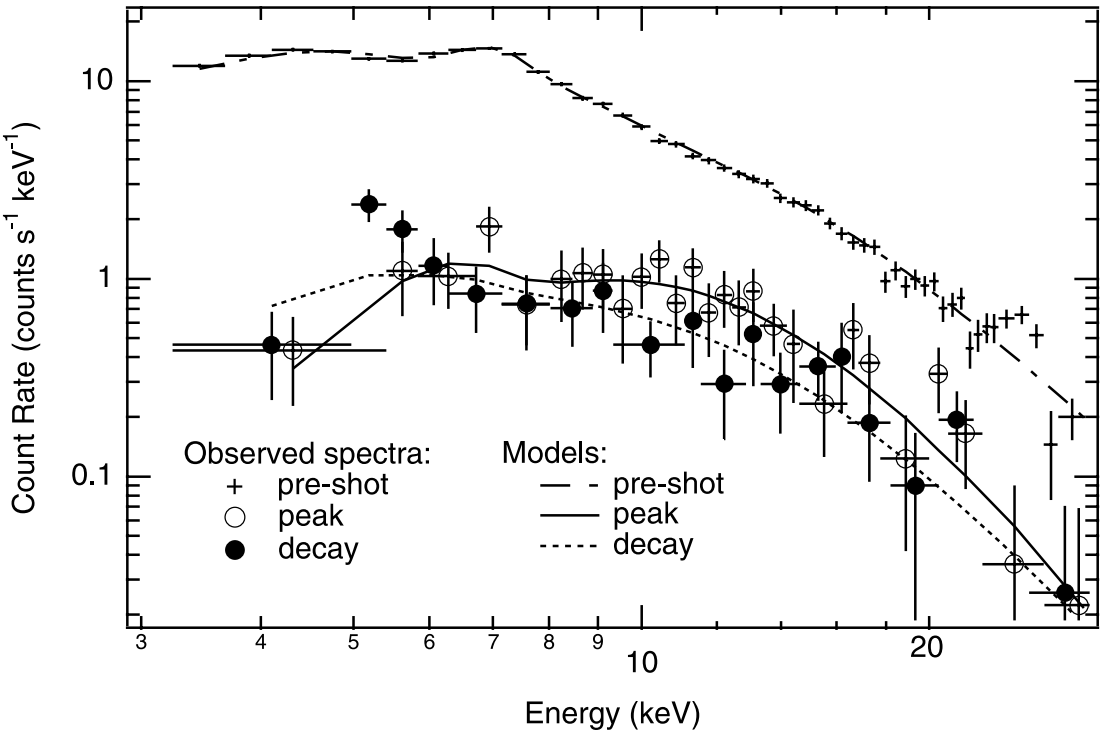

FIG. 5.—Spectra and best-fit models of the preshot phase (*crosses*), the peak phase (*open circles*), and the decay phase (*filled circles*). To emphasize the spectral evolution of the shot component, the preshot spectrum is subtracted from the peak and decay spectra. The background spectrum made with the tool `pcabackest` is subtracted from the preshot spectrum.

coincide with a massive jet ejection event, we further assume that they are related to the ejection in the following discussion.

Since the spectral fit is consistent with a decrease of the absorption hydrogen column density during the evolution of the shots, we attribute the rise of the shots to the decrease of attenuating matter, or in other words, the emergence of an X-ray–emitting small plasma bullet from behind the attenuating matter. Each shot corresponds to the shot of a small plasma bullet from the nozzle. This interpretation is different from that of the X-ray variability seen in GRS 1915+105, which is explained in terms of the rapid removal and replenishment of matter forming the inner part of an accretion disk (Belloni et al. 1997). Since both thermal and nonthermal spectral models are consistent with the observed spectrum, it is difficult to determine the emission mechanism. But in either case, physical quantities of the emitting bullets would be derived as follows.

3.3.3. *Thin-thermal Emission*

Given a spherical, thin-thermal, freely expanding plasma bullet with a temperature $T(t)$, a radius $R(t) = v_{\rm exp}t$, an expanding velocity $v_{\rm exp} = {\rm const}$, and a total number of electrons $N_e = {\rm const}$, the cooling would be governed by the equation

$$\frac{3}{2}(1+X)N_e k_{\rm B}\frac{dT}{dt} = -\frac{\Lambda(T)XN_e^2}{(4/3)\pi R^3} - 3(\gamma-1)\frac{3}{2}(1+X)N_e k_{\rm B}\frac{Tv_{\rm exp}}{R}, \quad (3)$$

where $X = N_i/N_e$ is the ratio of the total number of ions to that of electrons, assumed to be 0.93117; $k_{\rm B}$ is the Boltzmann constant; and γ is the adiabatic index, assumed to be 5/3. The first term on the right-hand side corresponds to radiative cooling, and the coefficient $\Lambda(T)$ is defined so that $\Lambda(T)N_e/(4\pi R^3/3)N_i/(4\pi R^3/3)$ equals the emitted power per unit volume. The last term corresponds to expansion: for expanding plasma with a volume $V(t)$,

$$V^{\gamma-1}dT = -T(\gamma-1)V^{\gamma-2}dV \quad (4)$$

is derived from the relation $TV^{\gamma-1} = {\rm constant}$. Substituting $V = 4\pi R^3/3$ in equation (4), the cooling rate by expansion, $dT/dt = -3(\gamma-1)Tv_{\rm exp}/R$, is obtained, which is equivalent to the last term of equation (3). The time parameter t is defined so that $t = 0$ at $R = 0$, although the radius can never be zero. If the coefficient $\Lambda(T)$ is proportional to $\sqrt{T}$ and written in the form $\Lambda(T) = \Lambda_T\sqrt{T}$, equation (3) has an analytic solution

$$\sqrt{T} = \left\{\sqrt{T_1} - \frac{\Lambda_T N_e X}{4\pi[7/2-(3/2)\gamma](1+X)k_{\rm B}v_{\rm exp}R_1^2}\right\}\left(\frac{R}{R_1}\right)^{-(3/2)\gamma+3/2} + \frac{\Lambda_T XN_e}{4\pi[7/2-(3/2)\gamma](1+X)k_{\rm B}v_{\rm exp}R_1^2}\left(\frac{R}{R_1}\right)^{-2} = \sqrt{T_1}\left[\left(1-\frac{L_1\tau_{\rm exp}}{2E_1}\right)\left(\frac{R}{R_1}\right)^{-1} + \frac{L_1\tau_{\rm exp}}{2E_1}\left(\frac{R}{R_1}\right)^{-2}\right], \quad (5)$$

$$E_1 = \frac{3}{2}(1+X)N_e k_{\rm B}T_1, \quad (6)$$

$$L_1 = \frac{3\Lambda_T\sqrt{T_1}XN_e^2}{4\pi R_1^3}, \quad (7)$$

$$\tau_{\rm exp} = \frac{R_1}{v_{\rm exp}}, \quad (8)$$

where the subscript "1" denotes the value at the peak; E_1, L_1, and $\tau_{\rm exp}$ correspond to the thermal energy, the luminosity of the bullet at the peak, and the timescale of expansion, respectively. The ratio $L_1\tau_{\rm exp}/(2E_1)$ represents the fraction of the thermal

energy in the bullet lost by radiation (cf. Kotani et al. 1996). Using equation (5), the luminosity of the bullet can be written as

$$L = L_1\left[\left(1-\frac{L_1\tau_{\rm exp}}{2E_1}\right)\left(\frac{R}{R_1}\right)^{-4}+\frac{L_1\tau_{\rm exp}}{2E_1}\left(\frac{R}{R_1}\right)^{-5}\right]. \quad (9)$$

The expansion velocity $v_{\rm exp}$ is estimated from the observed temperature as $v_{\rm exp}=[k_{\rm B}T_1/(\mu m_{\rm H})]^{1/2}=1.5^{+2.5}_{-0.6}\times10^8$ cm s^{-1}, where $m_{\rm H}$ is the mass of a hydrogen atom and μ is the mean molecular weight, assumed to be 0.587922. In 40 s, the luminosity of the plasma decreases by a factor of $1/e$. Substituting the factor into equation (9), we obtain

$$\frac{L_2}{L_1}=\frac{1}{e}=\left(1-\frac{L_1\tau_{\rm exp}}{2E_1}\right)\left(\frac{R_2}{R_1}\right)^{-4}+\frac{L_1\tau_{\rm exp}}{2E_1}\left(\frac{R_2}{R_1}\right)^{-5}, \quad (10)$$

where the subscript "2" denotes the value at the decay phase. Because the ratio of the radiation loss to the internal energy $L_1\tau_{\rm exp}/(2E_1)$ is between 0 and 1, the expansion in 40 s is constrained as $\exp\frac{1}{5}<R_2/R_1<\exp\frac{1}{4}$ from the above equation. Substituting $R_2=R_1+v_{\rm exp}\times40$ s, we obtain the radius as $R_1=2.2^{+3.6}_{-0.9}\times10^{10}$ cm. From this radius and an observed quantity L_1, all other parameters are derived; 1.06×10^2 s $<\tau_{\rm exp}<1.35\times10^2$ s, the number of electrons $N_e=1.0^{+2.1}_{-0.5}\times10^{45}$, the number density of electrons $n_{e,1}=4.1^{+9.2}_{-3.7}\times10^{13}$ cm^{-3}, and the thermal energy $E_1=0.7^{+13.7}_{-0.6}\times10^{38}$ ergs. Assuming that the bullet is moving at $0.26c$, the kinetic energy of the bullet is estimated to be $0.6^{+1.2}_{-0.3}\times10^{41}$ ergs. The assumption is consistent with the observed rise time of 20 s, which is naturally explained by the time it takes for a bullet to appear from a nozzle. Equation (5) is written with these estimates as

$$\sqrt{T}=\sqrt{14\ ({\rm keV})}\left\{0.3\left[\frac{R}{1.6\times10^{10}\ ({\rm cm})}\right]^{-1}+0.7\left[\frac{R}{1.6\times10^{10}\ ({\rm cm})}\right]^{-2}\right\}, \quad (11)$$

where errors are omitted.

Since a shot and the unmodulated component coexist, the bullets and the continuously emanating jet may coexist. In that case, the small plasma bullets can be interpreted as bright knots in the continuous jet. The knots are created when the mass outflow rate or the density of the continuous jet is temporarily increased. A temporal increase of temperature is not plausible because it would result in a change of the spectrum, which has not been observed. The properties of the knots would not be much different from those of the small plasma bullets discussed above, and the estimates above are valid if the knots or bullets coexist with the continuous jet.

3.3.4. *Synchrotron Emission*

Because the spectral shape does not change much in the decay and because no iron line is detected in the shot component, a nonthermal emission from expanding bullets also can account for the shot component. As for the steady nonvariable component, it is definitely a thin-thermal emission with Doppler-shifted iron lines. Therefore, it is natural to interpret the shot component as a thermal emission, and an interpretation of nonthermal emission is rather eccentric. In the following paragraph, we show physical parameters of a plasma bullet assuming that the bullets emit X-rays via synchrotron radiation.

A power-law distribution of synchrotron electrons,

$$f(\gamma)d\gamma \equiv \begin{cases}\dfrac{-p+1}{\gamma_{\rm max}^{-p+1}-1}n_{e,{\rm syn}}\gamma^{-p}d\gamma\approx(p-1)n_e\gamma^{-p}d\gamma, & 1<\gamma\le\gamma_{\rm max},\\ 0, & \gamma_{\rm max}<\gamma,\end{cases} \quad (12)$$

is assumed, where γ is the Lorentz factor of electrons, $n_{e,{\rm syn}}$ is the synchrotron electron number density, and $p=2.2^{+1.4}_{-1.0}$ is the electron energy index derived from the photon index $\Gamma=(p+1)/2$. The maximum Lorentz factor should be at least $\gamma_{\rm max}>1.4\times10^5$ to account for the X-ray emission up to 10 keV. Optically thin synchrotron flux from such a sphere is expressed as

$$F_\nu=\frac{\chi(p)}{4\pi}n_{e,{\rm syn}}\frac{e^3}{mc^2}B^{p/2+1/2}\left(\frac{4\pi mc\nu}{3e}\right)^{-p/2+1/2}\frac{4\pi R^3/3}{D^2}, \quad (13)$$

$$\chi(p)\equiv\frac{3^{1/2}2^{p/2-1/2}(p-1)}{(p+1)}\times\frac{\Gamma(p/4+19/12)\Gamma(p/4-1/12)\Gamma(p/4+5/4)}{\Gamma(p/4+7/4)}, \quad (14)$$

where ν is the frequency and B is the magnetic field strength in the plasma (e.g., Hjellming & Han 1995). By substituting the observed flux $F\nu(1\ {\rm keV})=1.0^{+1.0}_{-0.5}\times10^{-2}$ photons cm^{-2} s^{-1} keV^{-1} into equation (13), the magnetic field strength B and the total number of electrons in a bullet N_e are constrained as

$$\log\left[N_eB^{p/2+1/2}\ ({\rm G})\right]=44.6^{+3.0}_{-2.9}, \quad (15)$$

where the rather large uncertainty is due to the uncertainty of the electron energy index p.

As the bullet expands, each high-energy electron loses energy as $E=(R/R_1)^{-1}$ and the magnetic field and the luminosity decrease as $B=B_1(R/R_1)^{-2}$ and $L=L_1(R/R_1)^{-2p}$, respectively. Radiative cooling and heating are neglected. Thus, a decrease of flux by a factor of $1/e$ corresponds to an adiabatic expansion by $1.26^{+0.25}_{-0.10}$ of the radiating bullet. Further assuming that the bullet is proceeding at $0.26c$ with an expanding half-angle of $2\overset{\circ}{.}1$, which are the same value as the velocity and the half-opening angle of the continuous jet (Namiki et al. 2003), the expansion velocity is estimated as $v_{\rm exp}=2.9\times10^8$ cm s^{-1}. From this expansion velocity and the expansion factor obtained above, the radius of the plasma is determined as $R=(4.5\pm1.4)\times10^{10}$ cm, which is consistent with the rise time of 20 s.

The synchrotron electron number density and the strength of the magnetic field can be estimated if their energies are assumed to be in equipartition, i.e.,

$$\frac{B^2}{8\pi}=\int_1^{\gamma_{\rm max}}\frac{p-1}{\gamma_{\rm max}^{-p+1}-1}n_emc^2\gamma^{-p+1}d\gamma \quad (16)$$

$$\approx\begin{cases}\dfrac{p-1}{-p+2}\gamma_{\rm max}^{-p+2}n_emc^2, & 1<p<2,\\ \dfrac{p-1}{p-2}n_emc^2, & 2<p.\end{cases} \quad (17)$$

Substituting an electron energy index of $p = 2.2$, we obtain $B = 1.8 \times 10^2$ G and $n_e = 2.4 \times 10^8$ cm^{-3}. The total number of electrons and internal energy in a bullet are estimated as $N_e = 9 \times 10^{40}$ per shot and $E_{\rm syn} = 5.3 \times 10^{35}$ ergs, respectively. The numbers of electrons and internal energy derived here are smaller by orders of magnitude than those of the thin-thermal case.

3.3.5. *Comptonized Emission*

If the emission mechanism is inverse Compton scattering of optical photons, the seed photon density would decrease and the emission would decay as the plasma bullet gets away from the central engine. Based on this Comptonized emission model, the parameters of the plasma bullet, such as the electron number density, the total number of electrons, and the total energy of electrons, are estimated. They are found to be not much different from those in the case of synchrotron emission, although the uncertainties of parameters are larger in the case of inverse Comptonization.

3.4. *The Massive Jet*

Based on the bullets model, we suggest an explanation of the massive jet ejection: During the massive jet ejection event, small discrete plasma bullets, or knots in the continuously emanating flow, are successively ejected at random intervals of $\sim$150 s. The radius of bullets is estimated as $R_1 = 2.2^{+3.6}_{-0.9} \times 10^{10}$ cm. The X-ray emission from the small plasma bullets, either thermal or nonthermal, decays in 40 s as it expands. Assuming that the most active state lasts 3 days, the total number of small bullets ejected in a single massive jet event is estimated to be 1700. The total mass and total kinetic energy of all 1700 bullets are $3.3^{+6.7}_{-1.8} \times 10^{24}$ g and $1.0^{+2.1}_{-0.5} \times 10^{44}$ ergs, respectively. The average mass ejection rate and average kinetic luminosity over 3 days are $0.7^{+1.6}_{-0.4} \times 10^{16}$ g s^{-1} and $3.9^{+8.0}_{-2.1} \times 10^{38}$ ergs s^{-1}, respectively. In the case of synchrotron emission from baryonic plasma, only the lower limits of mass and kinetic energy are derived; the total mass and total kinetic energy of the 1700 bullets would be at least 3.0×10^{20} g and 9.1×10^{39} ergs, respectively, and the average mass ejection rate and average kinetic luminosity would be at least 1.1×10^{15} g and 3.5×10^{34} ergs s^{-1}, respectively.

The estimated average kinetic luminosity of $\sim 10^{38}$ ergs s^{-1} is considerably lower than estimates based on the quiescent or normal state. For example, Kotani (1997) has calculated the kinetic luminosity as 1×10^{40} ergs s^{-1} based on *ASCA* data, Marshall et al. (2002) as 3.2×10^{38} ergs s^{-1} based on *Chandra* HETGS data, and Brinkmann et al. (2005) as 5×10^{39} ergs s^{-1} based on *XMM-Newton* EPIC data. It is puzzling that the mass outflow rate and kinetic luminosity in the massive jet ejection are not so "massive" compared to those of the steady continuous jet flow seen on most occasions. There are several possibilities to account for the inconsistency in terms of the bullets model: (1) The mass outflow rate and kinetic luminosity of a massive jet are not larger than those of a quiescent steady jet, but the efficiency to accelerate electrons contributing to synchrotron radio emission is far larger. (2) The massive jet is not an assembly of the small plasma bullets but is mainly supplied with the steady flow that coexists with the bullets. (3) In spite of the monitoring observation with a sampling rate of 3 ks day^{-1}, we have missed the moment of the true massive jet ejection, which lasts only, say, hours, and a massive jet of 10^{44}–10^{45} ergs is ejected at a maximum outflow rate of 10^{40}–10^{41} ergs s^{-1}. We do not yet have any evidence supporting one of these scenarios, but we suggest that the second case is unlikely, in which the unvariable X-ray component is expected to rise as the radio flux densities rise.

Another question is whether X-ray variability is really related to radio flaring, which is associated with blob rebrightening events out of the system core. At 1.6 GHz, radio flares peak at 35 AU from the core (Paragi et al. 1999). If radio flares are caused by an environmental condition, it would not be detectable in the X-ray band at the ejection, and the coincidence of the rapid X-ray variability and the massive jet event would have been accidental. However, Paragi et al. (1999) suggest that the rebrightening is due to attenuation by out-flowing gas around the core. If the cause of radio flares is not an environmental condition but a core activity, the activity that changes the radio flux by a factor of 2 might be detectable in the X-ray band. That should be tested in future multiwavelength observations.

X-ray shots are first seen in the data from MJD = 52, 225, 1 week before its maximum activity and the onset of a second radio flare. Provided that shots precede a radio flare, we can predict a massive jet ejection event on the basis of X-ray monitoring data. Upon detection of X-ray shots, notice of a massive jet ejection to occur in 1 week can be sent to ground and space observatories. An observation campaign covering a massive jet ejection is possible. There is still a possibility that the duration of a massive jet ejection is shorter than 1 day and the moment has been missed even in our observations. This can be confirmed in future observations. In addition, this technique may be applicable for the prediction of massive jet ejections from other microquasars. In spite of numerous observations performed so far, it is not yet known whether massive jet ejections from other microquasars such as GRS 1915+105 are also preceded by a precursor or not. As a specially coordinated observation is required to detect the shotlike variability from SS 433, a carefully coordinated observation plan is desirable to observe GRS 1915+105 in a massive jet ejection event with an X-ray mission. The findings reported here imply that new and important physics of a microquasar is revealed by observing massive jet ejections. The observation of these events is essential to explore the nature of microquasars. Therefore, the technique for observing massive jet ejections is one of the most important results from this study. Future observations of massive jet ejections from microquasars are encouraged.

T. K. is supported by a 21st Century COE Program at Tokyo Tech, "Nanometer-Scale Quantum Physics," of the Ministry of Education, Culture, Sports, Science, and Technology. S. A. T. is very grateful to the Russian Base Researches Foundation for support of the SS 433 monitoring with the RATAN-600 radio telescope. K. K. is supported by Grant-in-Aid 16740121 from the Ministry of Education, Culture, Sports, Science, and Technology of Japan. We thank the anonymous referee for useful comments and suggestions to improve this paper.

REFERENCES

Band, D. 1989, ApJ, 336, 937
Belloni, T., Mendez, M., King, A. R., van der Klis, M., & van Paradijs, J. 1997, ApJ, 479, L145
Brinkmann, W., Kotani, T., & Kawai, N. 2005, A&A, 431, 575
Chakrabarti, S. K., Pal, S., Nandi, A., Anandarao, B. G., & Mondal, S. 2003, ApJ, 595, L45
Fender, R. P. 2001, in Proc. ESO Workshop, Black Holes in Binaries and Galactic Nuclei, ed. L. Kaper, E. P. J. van den Heuvel, & P. A. Woudt (Berlin: Springer), 193
Fiedler, R. L., et al. 1987, AJ, 94, 1244
Foster, R. S., et al. 1996, ApJ, 467, L81
Gies, D. R., McSwain, M. V., Riddle, R. L., Wang, Z., Wiita, P. J., & Wingert, D. W. 2002, ApJ, 566, 1069

Hasegawa, T., Malasan, H. L., Kawakita, H., Obayashi, H., Kurabayashi, T., Nakai, T., Hyakkai, M., & Arimoto, N. 2004, PASJ, 56, 295
Hjellming, R. M., & Han, X. 1995, in X-Ray Binaries, ed. W. H. G. Lewin, J. van Paradijs, & E. P. J. van den Heuvel (Cambridge: Cambridge Univ. Press), 308
Kawai, N. 1989, in Proc. 23rd ESLAB Symp. on Two Topics in X-Ray Astronomy, ed. N. E. White, J. J. Hunt, & B. Battrick (Noordwijk: ESA), 453
Kinugasa, K., et al. 2002, ApJ, 577, L97
Klein-Wolt, M., Fender, R. P., Pooley, G. G., Belloni, T., Migliari, S., Morgan, E. H., & van der Klis, M. 2002, MNRAS, 331, 745
Korolkov, D. V., & Pariiskii, I. N. 1979, S&T, 57, 324
Kotani, T. 1997, Ph.D. thesis, Univ. Tokyo
Kotani, T., Band, D., Denissyuk, E. K., Kawai, N., Kinugasa, K., Namiki, M., Safi-Harb, S., & Trushkin, S. 2002, in ASP Conf. Ser. 279, Exotic Stars as Challenges to Evolution, ed. C. A. Tout & W. Van Hamme (San Francisco: ASP), 19
Kotani, T., Kawai, N., Matsuoka, M., & Brinkmann, W. 1996, PASJ, 48, 619
Kotani, T., & Trushkin, S. 2001, IAU Circ. 7747
Kotani, T., Trushkin, S., Denissyuk, E. K., Kawakita, N., Kinugasa, K., Safi-Harb, S., & Band, D. 2003, in New Views on Microquasars, ed. P. Durouchoux, Y. Fuchs, & J. Rodriguez (Kolkata: Centre for Space Physics), 265
Marshall, H. L., Canizares, C. R., & Schulz, N. S. 2002, ApJ, 564, 941
Mirabel, I. F., Dhawan, V., Chaty, S., Rodriguez, L. F., Marti, J., Robinson, C. R., Swank, J., & Geballe, T. 1998, A&A, 330, L9
Mirabel, I. F., & Rodríguez, L. F. 1994, Nature, 371, 46
———. 1999, ARA&A, 37, 409
Mironov, A. V., & Tereshchenko, V. M. 1998, Baltic Astron., 7, 351
Muno, M. P., Remillard, R. A., Morgan, E. H., Waltman, E. B., Dhawan, V., Hjellming, R. M., & Pooley, G. 2001, ApJ, 556, 515
Namiki, M., Kawai, N., & Kotani, T. 2001, in ASP Conf. Ser. 251, New Century of X-Ray Astronomy, ed. H. Inoue & H. Kunieda (San Francisco: ASP), 390
Namiki, M., Kawai, N., Kotani, T., & Makishima, K. 2003, PASJ, 55, 281
Paragi, Z., Vermeulen, R. C., Fejes, I., Schilizzi, R. T., Spencer, R. E., & Stirling, A. M. 1999, A&A, 348, 910
Revnivtsev, M., et al. 2004, A&A, 424, L5
Safi-Harb, S. 1997, Ph.D. thesis, Univ. Wisconsin
Safi-Harb, S., & Kotani, T. 2003, in New Views on Microquasars, ed. P. Durouchoux, Y. Fuchs, & J. Rodriguez (Kolkata: Centre for Space Physics), 279
Trushkin, S. A., Bursov, N. N., & Nizhelskij, N. A. 2003, Bull. Spec. Astrophys. Obs., 56, 57
Ueda, Y., et al. 2002, ApJ, 571, 918
Vermeulen, R. C., Schilizzi, R. T., Spencer, R. E., Romney, J. D., & Fejes, I. 1993, A&A, 270, 177
Yuan, W., Kawai, N., Brinkmann, W., & Matsuoka, M. 1995, A&A, 297, 451